electrochem

MDPI

Article

An Experimental and Theoretical Investigation of the Efficacy of Pantoprazole as a Corrosion Inhibitor for Mild Steel in an Acidic Medium

Avni Berisha

Department of Chemistry, Faculty of Natural and Mathematics Science, University of Prishtina, 10000 Prishtina, Kosovo; avni.berisha@uni-pr.edu

Abstract: The corrosion behavior of mild steel in a 1 M aqueous sulfuric acid medium in the presence and absence of the drug Pantoprazole was investigated using potentiodynamic polarization and quantum chemical calculations as well as Monte Carlo and molecular dynamic simulations. The potentiodynamic experiments indicated that this molecule, as a result of its adsorption on a mild steel surface, functioned as a mixed inhibitor. The goal of the study was to use theoretical calculations to acquire a better understanding of how inhibition works. The adsorption behavior of the examined compounds on the Fe (1 1 0) surface was calculated using a Monte Carlo simulation. Furthermore, the molecules were studied using density functional theory (DFT), especially the PBE functional, to determine the relationship between the molecular structure and the corrosion inhibition behavior of the chemical under research. The adsorption energies of Pantoprazole (in its three different protonation states) iron were calculated more precisely using molecular mechanics with periodic boundary conditions (PBC). The predicted theoretical parameters were found to be in agreement with the experimental data, which was a considerable help in understanding the corrosion inhibition mechanism displayed by this chemical.

Keywords: corrosion inhibition; Pantoprazole; Tafel plots; DFT; MC; MD

Citation: Berisha, A. An Experimental and Theoretical Investigation of the Efficacy of Pantoprazole as a Corrosion Inhibitor for Mild Steel in an Acidic Medium. *Electrochem* **2022**, *3*, 28–41. https://doi.org/10.3390/electrochem3010002

Academic Editor: Masato Sone

Received: 11 December 2021
Accepted: 4 January 2022
Published: 6 January 2022

1. Introduction

The physical and chemical properties of mild steel as well as its availability and cost have made it one of the most extensively utilized materials in a wide range of industrial fields [1–6]. This material is used in a range of applications, including mineral processing equipment, petroleum refining, and other building materials. Despite having a wide range of uses, the material has a low corrosion resistance when subjected to different atmospheric conditions. Many metal materials degrade as a result of this exposure, resulting in substantial economic consequences. As a result, corrosion prevention and protection have become unavoidable requirements. Several methods have been explored to protect metals but one of the most successful and cost-effective has been the inclusion of inhibitors into the corrosion media. According to the literature, the most efficient corrosion inhibitors are organic molecules containing unsaturated bonds, aromatic rings, and heteroatoms such as O, N, and S [7–10]. Using mild steel in 1 M H_2SO_4, we investigated the inhibitory impact of the drug Pantoprazole [6-(difluoromethoxy)-2-(((3,4-dimethoxypyridin-2-yl)methyl)sulfinyl)-1H-benzo[d]imidazole] on the corrosion of this material. This drug is a possible corrosion inhibitor due to its chemical structure, which contains heteroatoms (O, N, S, F) and numerous double bonds. Theoretical calculations (DFT, MC, and MD) were used to complete the experimental study.

2. Materials and Methods

2.1. Instrument, Material, Electrode Preparation, and the Corrosive Solution

A PalmSens3 potentiostat was used in combination with a three-electrode cell at 298 K. A graphite rod (d = 3 cm, l = 4 cm) was employed as an auxiliary electrode, and a saturated calomel electrode (SCE) was used as a reference electrode. Scanning the electrode potential vs. E_{OCP} at a 1 mV/s sweep rate yielded potentiodynamic polarization curves. The measurements were taken in an atmospheric environment. To guarantee reproducibility, each experiment was carried out three times. Table 1 shows the mass percentages of mild steel (in weight percent) [11]. The corrosive solution utilized was a 1 M sulfuric acid solution that was prepared by diluting the solution with bi-distilled water.

Table 1. Composition of mild steel (in %).

Fe	C	P	Mn	Si	Cr	S	Mo	Ni
99.54	0.1252	0.0316	0.1836	0.0561	0.0124	0.0282	0.0125	0.0015

The electrode for the electrochemical studies was created by embedding a mild steel rod (d = 1.6 mm, l = 12 cm) into a Teflon® tube (d = 0.8 cm, l = 10 cm) using epoxy glue and allowing it to cure. The electrode was polished on silicon carbide abrasive paper with a medium grain diameter of 6.5–15.3 microns, then on a (DP-Nap) cloth soaked in an aluminum oxide solution with a particle size of 0.3 microns, then rinsed and sonicated in water.

2.2. DFT Calculations

The DFT calculations were fulfilled by Dmol3 software from Biovia [12,13]. A meta-generalized gradient approximation [14,15] employing M11-L [15–17] and a double numeric quality basis set (DNP) [18] were used for the geometry optimizations. A lower than 0.00001 kcal/mol convergence standard for the self-consistent field (SCF) was used for the SCF. The energy minima were validated by carrying out a vibrational analysis and establishing that there were no imaginary frequencies present in the data [19–21].

2.3. Monte Carlo (MC) and Molecular Dynamic (MD) Simulation

The simulation of the interaction of a mild steel surface with the drug Pantoprazole was performed in a corrosion environment by utilizing a ten atom-thick layer unit cell of Fe (1 1 0) surface as the basis for the experiment (under a periodic boundary condition). The sizes of the slab model were 19.859 Å × 19.859 Å × 18.342 Å with an enclosed addition of a 30 Å vacuum layer at the C axis that was introduced with 1 Pantoprazole molecule/350 H_2O molecules/5 sulphate + 10 hydronium ions. In advance of the MD step, the geometry of the simulation boxes was optimized (energy converge tolerance of 1×10^{-5} kcal/mol) using the Forcite module in the Biovia software package.

MD was performed at a temperature of 25 °C [22] using the constant volume/constant temperature (NVT) canonical ensemble with a simulation period of 1000 ps [23–27]. The Berendsen thermostat conserved the temperature. The calculations for MC and MD were carried out using the Condensed Phase Optimized Molecular Potential II (COMPASSII) forcefield [26,28–36]. A radial distribution function (RDF) analysis included the entire MD trajectory [2,20,21,23].

3. Results

3.1. Polarization Measurements

The anodic and cathodic polarization curves of a mild steel electrode in a 1 M H_2SO_4 solution are shown in Figure 1 in the absence and presence of the drug Pantoprazole at 298 K. The *IE* (in percent) was determined using Equation (1):

$$IE(\%) = \frac{i^{corr.}_{absence\ of\ inhibitor} - i^{corr.}_{presence\ of\ inhbitor}}{i^{corr.}_{absence\ of\ inhibitor}} 100\ . \quad (1)$$

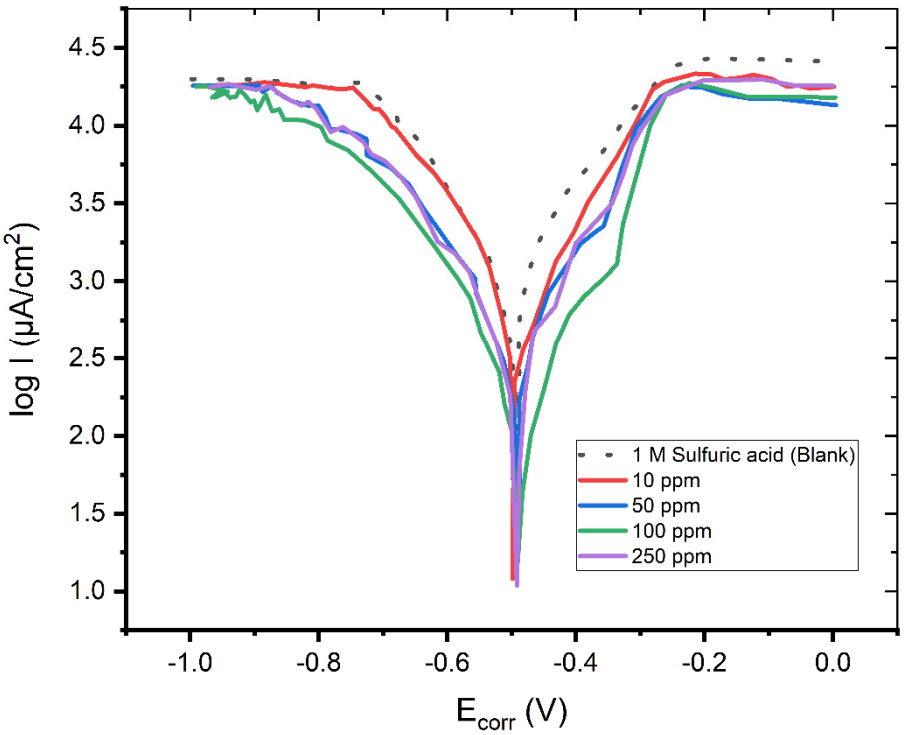

Figure 1. The Tafel plot of the mild steel electrode measured in a H_2SO_4 solution (c = 1 M) in the absence and in the presence of 10, 50, 100, and 250 ppm of Pantoprazole.

The electrochemical parameters of the corrosion potential (E_{corr}) and corrosion current density (i_{corr}) were determined from the intersection of the anodic and cathodic Tafel slopes and are presented in Table 2.

Table 2. Electrochemical parameters of mild steel at various concentrations of Pantoprazole molecules in 1 M sulfuric acid.

C (ppm)	E_{corr} (V)	I_{corr} (µA/cm²)	bc (mV/dec)	ba (mV/dec)	*IE* (%)
-	−0.502	0.4891	−153.1	84.4	-
10	−0.480	0.2908	−155.2	92.1	48.34
50	−0.491	0.1933	−166.1	96.4	72.12
100	−0.495	0.1689	−166.9	98.1	78.27
250	−0.472	0.1014	−172.2	99.4	94.53

The Tafel plot in Figure 1 reveals that the adsorption of the Pantoprazole molecules onto the mild steel surface significantly reduced the corrosion current of the mild steel in this hostile environment, indicating a high degree of corrosion inhibition of up to 94.53 percent.

When Pantoprazole was present in the solution, the values of the cathodic and anodic Tafel slopes (bc, ba) changed. The changes in the Tafel slopes indicated that the molecule

had an effect on the kinetics of the hydrogen evolution process [10]. This resulted in a greater energy barrier for the proton discharge and, therefore, less gas evolution. The investigated compound had no discernible effect on the corrosion potential, suggesting that it acted as mixed-type inhibitor [6].

3.2. DFT, MC, and MD Results

The microspecies distribution of the Pantoprazole molecules was performed using Chemaxon software prior to the computation to take into consideration the pH influence on the protonation/deprotonation of the Pantoprazole molecule. As may be observed in Figure 2A, Form A, C, and E of the chemical structures were below a pH of 7.

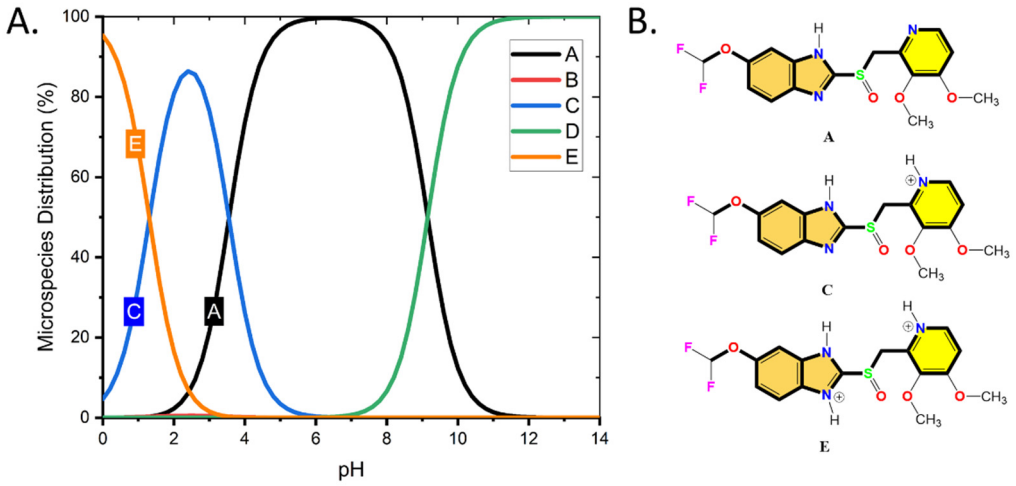

Figure 2. (**A**) The distribution percentage of Pantoprazole molecular forms vs. the pH value of the media and (**B**) three major species distributed at pH < 7 used in the theoretical calculations (DFT, MC, and MD).

According to [37,38], charge density profiles are seen as a map of the charge density distribution across the surface of the molecule and give information about the molecule as well as information about its solubility. To create the charge density curve, referred to as the sigma profile, it is essential to perform calculations centered on the conductor-like screening model (COSMO) (Figure 3). COSMO operates on molecular-shaped cavities, which are characterized by partial atomic charges and serve as a representation of the electrostatic potential [15,39–42]. As seen in Figure 3 (peaks in the σ-profile at the screen charge density values near −0.01 and 0.01 e/Å^2), the inhibitors operated as an acceptor/donor of H-bonds in the process. As a result, the solubility of the various protonated forms of Pantoprazole was dependent on its capacity to interact with water molecules via this type of contact.

When it comes to molecular simulations and mechanism verifications, both HOMO and LUMO (Figure 4) are frequently employed as recommendations to determine if a reaction occurs normally and which components of the molecules are responsible for the reaction [6,29,30]. The HOMO displayed the electrons being donated to the electron-accepting portions of the molecule and the LUMO illustrated the electrons being donated to the net-donor sections of the molecule.

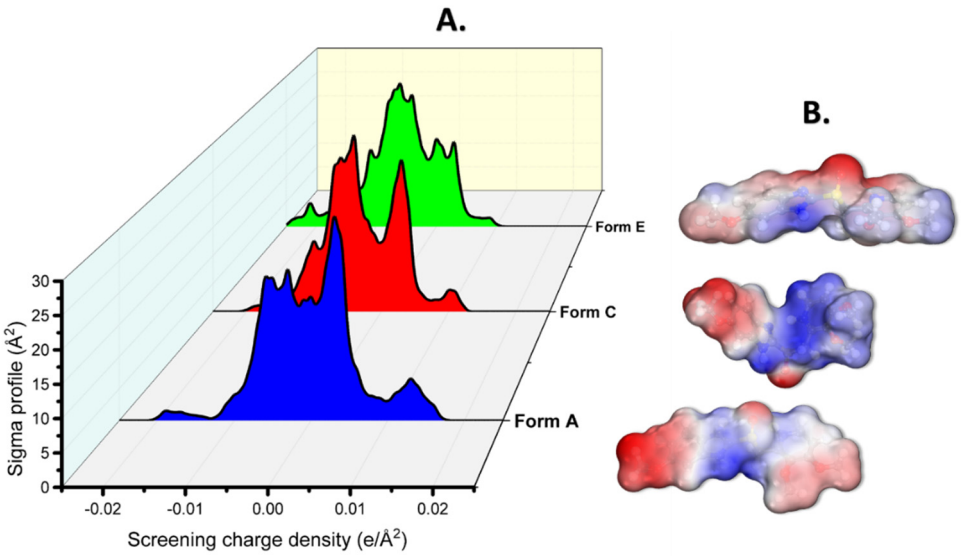

Figure 3. The (**A**) σ-profile and (**B**) 3D COSMO surface for the different protonated forms of a Pantoprazole molecule.

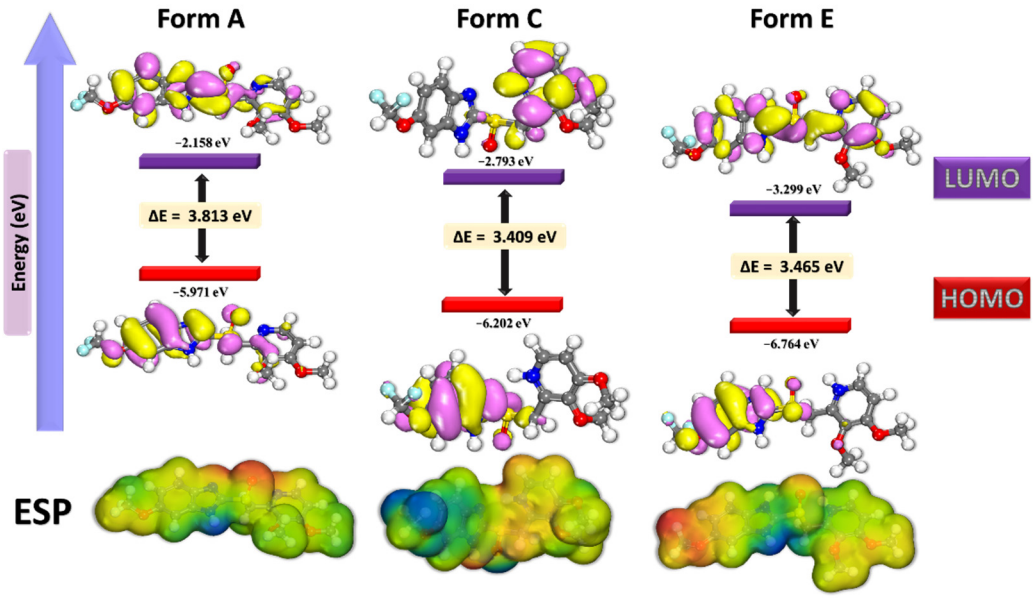

Figure 4. HOMO and LUMO surfaces as well as the electrostatic potential (ESP) for different protonated forms of a Pantoprazole molecule.

Figure 4 depicts the HOMO and LUMO OM and ESP of the Pantoprazole medication, and Table 3 lists the most often seen DFT indices. The majority of the HOMO and LUMO densities were localized in the region of the molecule that contained the imidazole moiety. When it comes to Pantoprazole, the HOMO and LUMO were significant due to their ability to interact with the Fe (1 1 0) surface via electron donation and acceptation, respectively [2,7,21,24–27,29–31,36,43–45].

When the electron affinity and ionization potential of the material were computed, a comparable capacity was obtained. Additionally, the proclivity of the forms of Pantoprazole for adsorption on metal surfaces were enhanced by an appropriate softness value and a relatively low hardness ratio [9,11,46,47].

Table 3. Calculated theoretical chemical parameters for the different protonated forms of the Pantoprazole inhibitor.

Theoretical Parameters	Pantoprazole Form A	Pantoprazole Form C	Pantoprazole Form E
HOMO	−5.9710	−6.2020	−6.7640
LUMO	−2.1580	−2.7930	−3.2990
ΔE (HOMO-LUMO)	3.813	3.409	3.465
Ionization energy (I)	5.9710	6.2020	6.7640
Electron affinity A)	2.1580	2.7930	3.2990
Electronegativity (X)	4.0645	4.4975	5.0315
Global hardness (η)	1.9065	1.7045	1.7325
Chemical potential (π)	−4.0645	−4.4975	−5.0315
Global softness (σ)	0.5245	0.5867	0.5772
Global electrophilicity (ω)	4.3326	5.9336	7.3062
Electrodonating (ω−) power	6.6032	8.3954	10.0385
Electroaccepting(ω+) power	2.5387	3.8979	5.0070
Net electrophilicity (Δω±)	2.3872	3.7788	4.9074
Fraction of transferred electrons (ΔN)	−0.2189	−0.3718	−0.5199
Energy from Inhib to Metals (ΔN)	0.0913	0.2356	0.4683
ΔE back-donation	−0.4766	−0.4261	−0.4331

3.3. MC and MD Results

As seen in Figure 5, the lowest energy configurations of the distinct protonated forms of the Pantoprazole molecule on the metal surface in the simulated corrosion environment were identified. It appeared that the heteroatoms (mostly oxygen and nitrogen atoms) were involved in the adsorption process of the inhibitor based on the adsorption geometries. The creation of a protective anticorrosion layer on the metal surface was a result of this adsorption affinity.

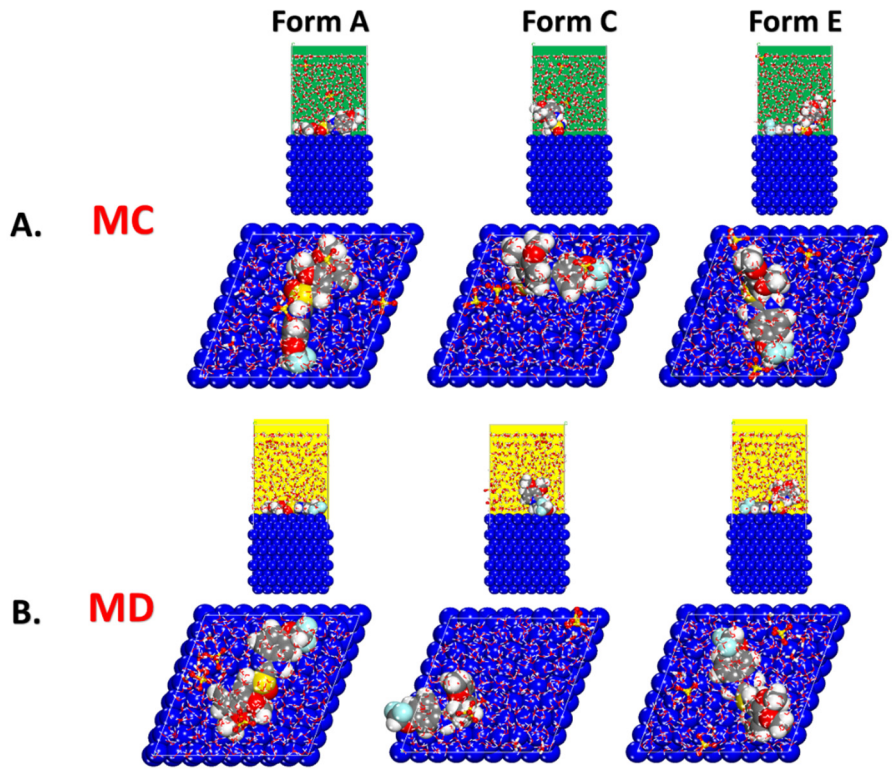

Figure 5. (**A**) MC and (**B**) MD obtained from the adsorption configurations of the different protonated forms of the Pantoprazole inhibitor in the simulated corrosion media on the Fe surface.

The quantitative determination of the interaction of the inhibitor molecule with the metal surface was accomplished via the computation of the adsorption energies using the following equation [48]:

$$E_{adsorption} = E_{Fe(110)|inhibitor} - \left(E_{Fe(110)} + E_{inhibitor}\right) \quad (2)$$

where $E_{Fe(110)\,|\,inhibitor}$ is the total energy of the simulated corrosion system and $E_{Fe(110)}$ and $E_{inhibitor}$ are the total calculated energy of the Fe (1 1 0) surface and that of the free inhibitor molecule, respectively.

For each MC, random molecular configurations as large as possible (ions or molecules) were chosen and deposited in the simulation box. Using the graph in Figure 6, we observed that when more of these systems were used, the average energy of the system approached a plateau, indicating that the system had reached its maximum energy balance (after 200,000 steps).

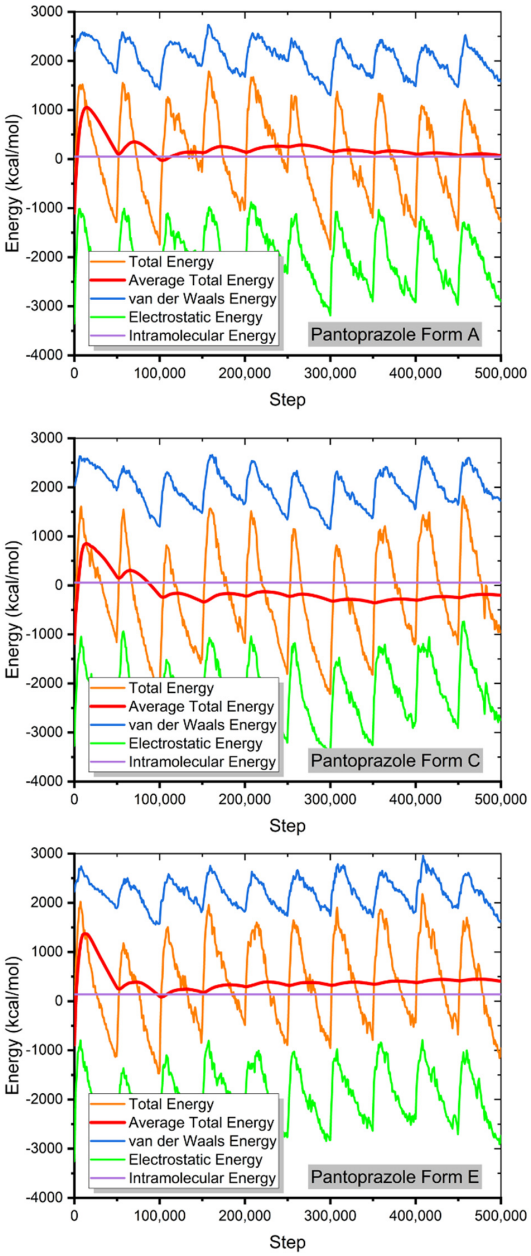

Figure 6. The contribution of the different energy terms during the MC calculations.

The results of the Monte Carlo simulations were consistent with those of the experiments. Due to the strong negative value of the adsorption energies (as seen in Figure 7), the adsorption process was considered to be spontaneous [11,24,25,33].

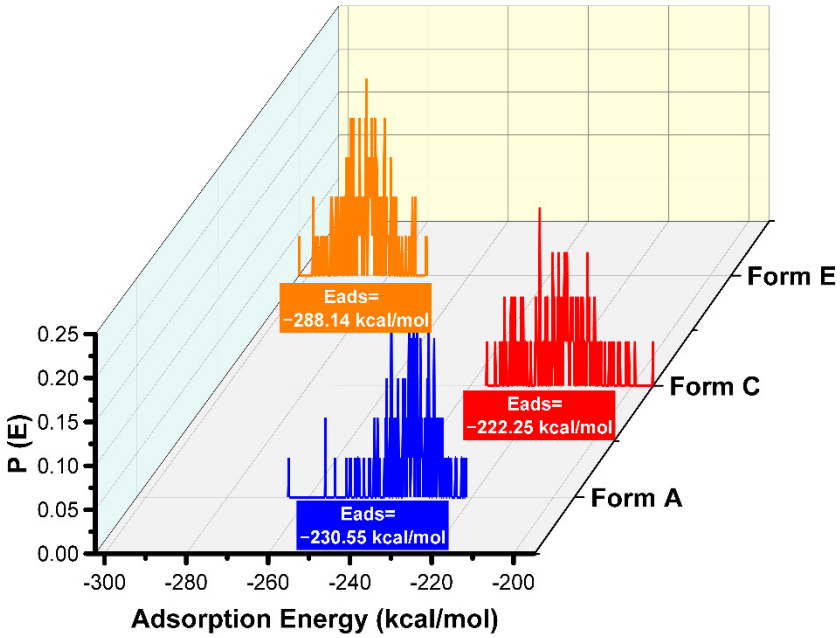

Figure 7. Distribution of the adsorption energies for the different protonated forms of the Pantoprazole inhibitor on to the iron surface obtained via MC.

It is possible to watch and record the dynamics of the adsorption of an inhibitor on metal surfaces using MD simulations [30]. Monitoring the actual temperature change during the MD run is one method to ensure that the system uses the least amount of energy. From Figure 8, it can be seen that the temperature drift was modest, suggesting that the MD of our system was successfully conducted.

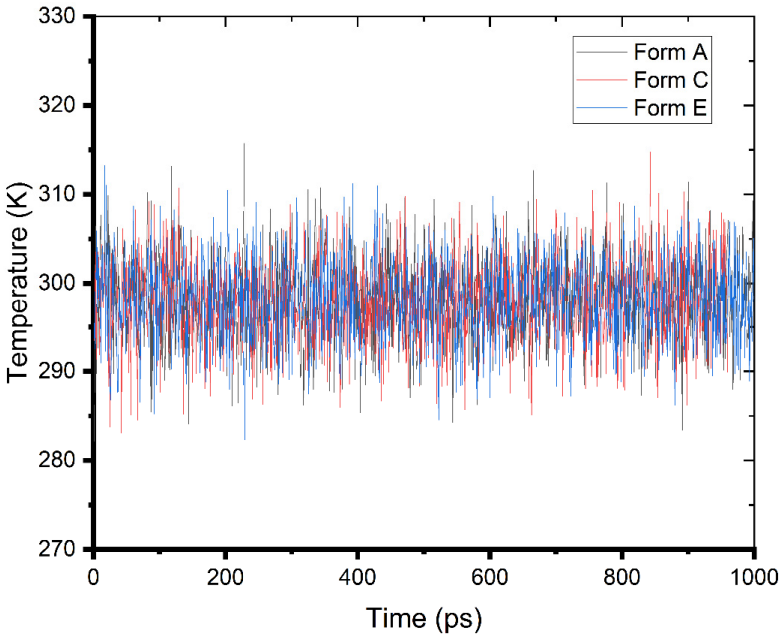

Figure 8. Temperature fluctuation (T = 298 K) during the MD run in the simulated corrosion media.

Figure 5 depicts the most recent inhibitor configurations on a metal surface. In accordance with the MC calculations, the N and O atoms were responsible for the adsorption of the Pantoprazole molecule. Using the adsorption energy calculated from the MD simulations (Figure 9), we observed that the inhibitor, regardless of its protonation form (A, C, or E), interacted strongly with the surface; it laid nearly flat on it, limiting the ability of the corrosion species to reach the surface, consequently reducing the severity and rate of the mild steel corrosion.

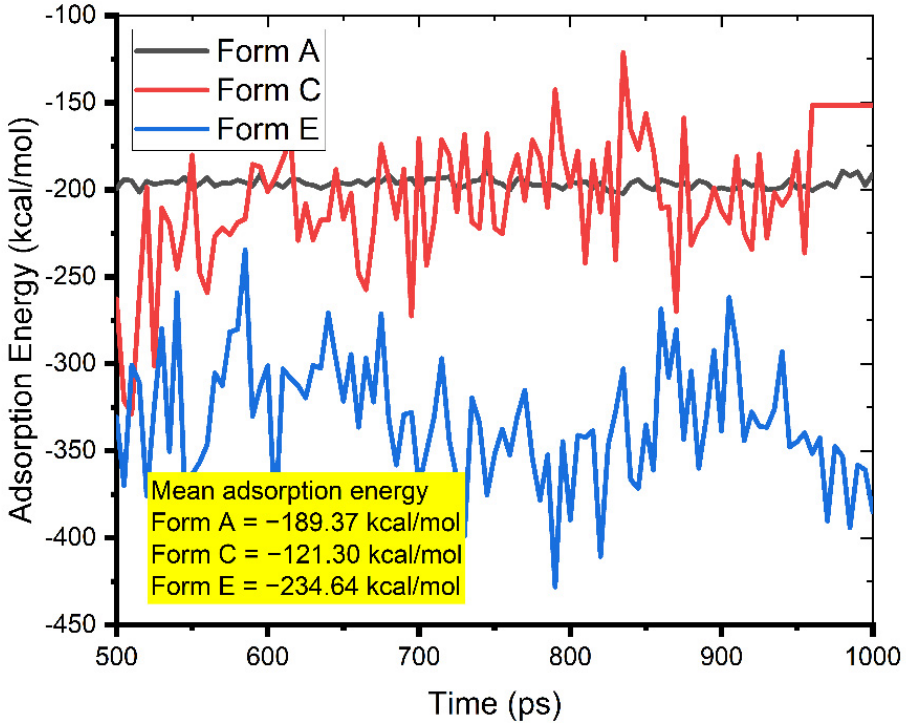

Figure 9. Evolution of the adsorption energy during the MD run in the simulated corrosion media during the interaction of Pantoprazole (Form A, C, and E) with the Fe (1 1 0) surface in the simulated corrosion media (the corresponding mean values of the interaction energies are presented in the graph).

This deduction was also sustained by the analysis of the radial distribution function (RDF), which calculated the oxygen atoms from the horizontal of the metal surface presented in Figure 10.

It has been commonly established that when a peak appears in the RDF graph of a particular atom(s) and the surface between 1 and 3.5 Å, it is a strong indication that chemisorption occurred whereas the presence of physisorption RDF peaks is estimated at greater distances (typically > 3.5 Å) [22,23,25,31–34,43].

The RDF for the O, N, S, and F atoms (Figure 10) of the inhibitor advocated the chemisorption of the inhibitor on the metal surface [28,29]. The accomplished results from MD and the corresponding RDF analysis validated the well-founded propensity of the inhibitors to adsorb and protect the metal.

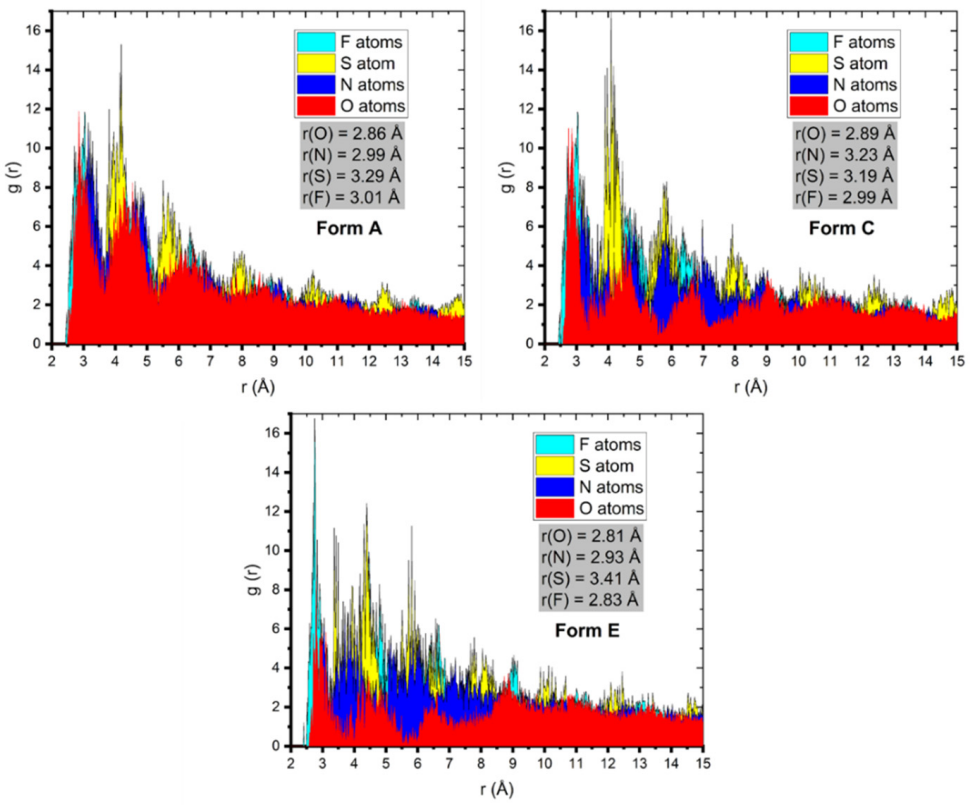

Figure 10. RDF oxygen, nitrogen, fluorine, and sulfur atoms for the Pantoprazole inhibitor onto the Fe (1 1 0) surface gained via MD.

3.4. The Study of the Film Density and the Self-Diffusion Coefficients of Pantoprazole

After 1000 ps of MD, the density values of the Pantoprazole-formed films were obtained; the average density values are presented in Table 4.

Table 4. Parameters for the corrosion thin-film model construction.

Pantoprazole	a = b = c (Å)	α = β = γ (°)	Density (g/cm^3)	Number of Molecules	Number of Particles
Form A	31.814	90	1.407	50	1
Form C	31.842	90	1.382	50	1
Form E	31.869	90	1.425	50	1

The fractional free volume (FFV) of the inhibitor films were evaluated from the free and the occupied volumes of the Connolly surface using the following equation [29]:

$$FFV = \frac{V_{free}}{V_{free} + V_{occupied}} \quad (3)$$

where V_{free} is the free volume and $V_{occupied}$ is the occupied volume of the PBC box containing the inhibitor film.

The determination of the self-diffusion coefficient (SDC) was calculated by [29]:

$$D = \frac{1}{6} \lim_{t \to \infty} \sum_{i=1}^{N\alpha} \langle \langle r_i(t) - r_i(0) \rangle^2 \rangle \quad (4)$$

where $\langle \langle r_i(t) - r_i(0) \rangle^2 \rangle$ is the mean squared displacement (MSD) values obtained from the MD trajectory (Figure 11).

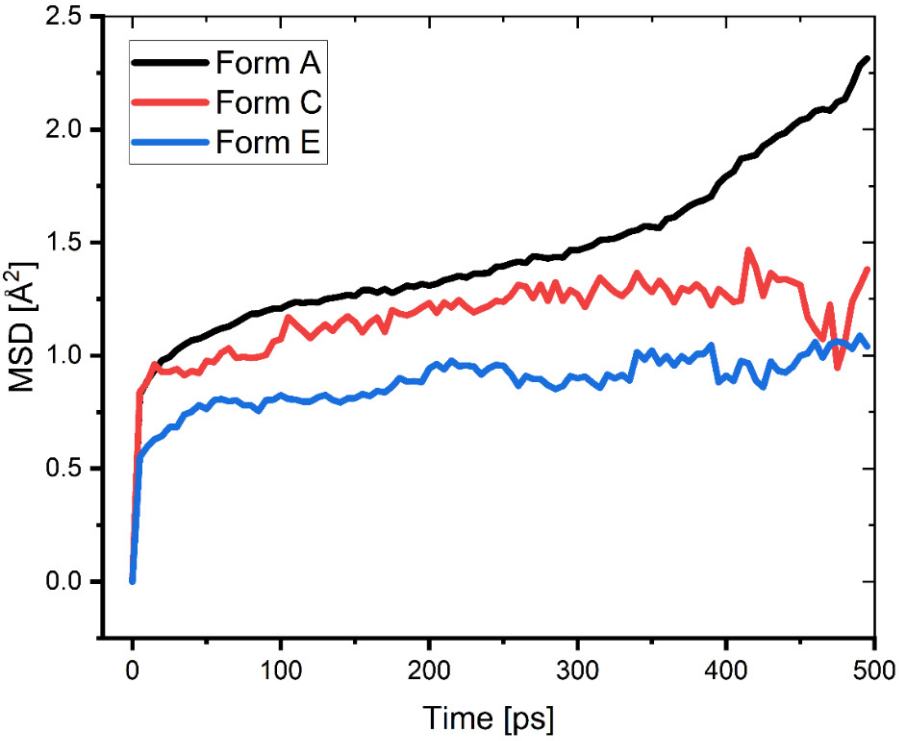

Figure 11. MSD of the different protonated forms of the Pantoprazole inhibitor during the second half of the MD simulation.

The FFV of the corrosive simulation media was calculated and is shown with other parameters in Table 5.

Table 5. Parameters for the corrosion thin-film model construction.

Pantoprazole	Form A	Form C	Form E
(Self-diffusion coefficient) (cm^2/s)	2.67×10^{-7}	1.16×10^{-8}	8.33×10^{-9}
Free volume ($Å^3$)	2814.56	3288.26	2276.13
Occupied volume ($Å^3$)	20,010.63	19,868.82	20,180.50
FFV	0.123309	0.141998	0.101357

An important characteristic that determines the mobility of corrosive ions (such as hydronium and sulphate ions) at the interface of a produced inhibitor film is the mobility of the inhibitors themselves. van der Waals and Coulomb forces work on the film-forming inhibitor molecules, causing them to interact and become displaced in the corrosive solution. This causes the volume and shape of the cavities in the film to change as well as the size of the cavities [29,48]. This has an effect on the mobility of the corrosive ions within the film. A high mobility film suggests that the corrosive species has a higher diffusion coefficient than normal. It was proposed that the SDC be used to assess the mobility of the inhibitor film. The self-diffusion coefficients for the Pantoprazole (Form A, C, and E) inhibitors are shown in Table 5. These values were determined by the balance between the flexibility of the molecule and its capacity to interact with nearby molecules in the surrounding environment. Although the protonation appeared to have no effect on the tight packing of Pantoprazole, this actually strengthened the interactions between its molecules. The reflection of the inhibitory performance of an inhibitor molecule is a complicated process that is the result of an accumulation of a number of different combined effects (volume of the molecule, adsorption ability, adsorption energy, the FFV of the film, the mobility of the film-forming molecules, the interaction of the corrosive species with the film, etc.).

4. Conclusions

The investigated compound was an effective mild steel inhibitor when used in an acidic environment. Using polarization measurements, it was discovered that this compound functioned as a mixed inhibitor. The adsorption centers of the inhibitors were determined by the use of DFT simulations. The MC and MD simulations further confirmed the strong adsorption contact of the inhibitor with the metal surface, giving molecular proof of the adsorption behavior (geometry) and adsorption energy of the Pantoprazole molecule on the iron surface, which was consistent with previous findings. Several theoretical results (DFT, MC, and MD) confirmed the results of the experiments.

Funding: This research received no external funding.

Institutional Review Board Statement: Not applicable.

Informed Consent Statement: Not applicable.

Data Availability Statement: Data available in a publicly accessible repository.

Acknowledgments: A.B. acknowledges the support from the Ministry of Education, Science and Technology of Kosovo (Nr.2-5069).

Conflicts of Interest: The author declares no conflict of interest.

References

1. Yilmaz, N.; Fitoz, A.; Ergun, Ü.; Emregül, K.C. A combined electrochemical and theoretical study into the effect of 2-((thiazole-2-ylimino)methyl)phenol as a corrosion inhibitor for mild steel in a highly acidic environment. *Corros. Sci.* **2016**, *111*, 110–120. [CrossRef]
2. Rbaa, M.; Ouakki, M.; Galai, M.; Berisha, A.; Lakhrissi, B.; Jama, C.; Warad, I.; Zarrouk, A. Simple preparation and characterization of novel 8-Hydroxyquinoline derivatives as effective acid corrosion inhibitor for mild steel: Experimental and theoretical studies. *Colloids Surf. A Physicochem. Eng. Asp.* **2020**, *602*, 125094. [CrossRef]
3. Lgaz, H.; Salghi, R.; Chaouiki, A.; Shubhalaxmi; Jodeh, S.; Bhat, K.S. Pyrazoline derivatives as possible corrosion inhibitors for mild steel in acidic media: A combined experimental and theoretical approach. *Cogent Eng.* **2018**, *5*, 1441585. [CrossRef]
4. Odewunmi, N.A.; Jafar Mazumder, M.A.; Ali, S.A.; Aljeaban, N.A.; Alharbi, B.G.; Al-Saadi, A.A.; Obot, I.B. Impact of Degree of Hydrophilicity of Pyridinium Bromide Derivatives on HCl Pickling of X-60 Mild Steel: Experimental and Theoretical Evaluations. *Coatings* **2020**, *10*, 185. [CrossRef]
5. Berisha, A.; Podvorica, F.; Mehmeti, V.; Syla, F.; Vataj, D. Theoretical and experimental studies of the corrosion behavior of some thiazole derivatives toward mild steel in sulfuric acid media. Maced. *J. Chem. Chem. Eng.* **2015**, *34*, 287–294. [CrossRef]
6. Al-Amiery, A.A.; Kadhum, A.A.H.; Alobaidy, A.H.M.; Mohamad, A.B.; Hoon, P.S. Novel Corrosion Inhibitor for Mild Steel in HCl. *Materials* **2014**, *7*, 662–672. [CrossRef]
7. Hsissou, R.; Benhiba, F.; Echihi, S.; Benkhaya, S.; Hilali, M.; Berisha, A.; Briche, S.; Zarrouk, A.; Nouneh, K.; Elharfi, A. New epoxy composite polymers as a potential anticorrosive coating for carbon steel in 3.5% NaCl solution: Experimental and computational approaches. *Chem. Data Collect.* **2021**, *31*, 100619. [CrossRef]
8. Rbaa, M.; Dohare, P.; Berisha, A.; Dagdag, O.; Lakhrissi, L.; Galai, M.; Lakhrissi, B.; Touhami, M.E.; Warad, I.; Zarrouk, A. New Epoxy sugar based glucose derivatives as eco friendly corrosion inhibitors for the carbon steel in 1.0 M HCl: Experimental and theoretical investigations. *J. Alloys Compd.* **2020**, *833*, 154949. [CrossRef]
9. Mehmeti, V.V.; Berisha, A.R. Corrosion study of mild steel in aqueous sulfuric acid solution using 4-methyl-4h-1,2,4-triazole-3-thiol and 2-mercaptonicotinic acid-an experimental and theoretical study. *Front. Chem.* **2017**, *5*, 61. [CrossRef] [PubMed]
10. Delley, B. From molecules to solids with the DMol3 approach. *J. Chem. Phys.* **2000**, *113*, 7756–7764. [CrossRef]
11. Andzelm, J.; King-Smith, R.D.; Fitzgerald, G. Geometry optimization of solids using delocalized internal coordinates. *Chem. Phys. Lett.* **2001**, *335*, 321–326. [CrossRef]
12. Perdew, J.P.; Burke, K.; Ernzerhof, M. Generalized gradient approximation made simple. *Phys. Rev. Lett.* **1996**, *77*, 3865–3868. [CrossRef]
13. Berisha, A. Interactions between the aryldiazonium cations and graphene oxide: A DFT study. *J. Chem.* **2019**, *2019*, 5126071. [CrossRef]
14. Mardirossian, N.; Head-Gordon, M. Thirty years of density functional theory in computational chemistry: An overview and extensive assessment of 200 density functionals. *Mol. Phys.* **2017**, *115*, 2315–2372. [CrossRef]
15. Inada, Y.; Orita, H. Efficiency of numerical basis sets for predicting the binding energies of hydrogen bonded complexes: Evidence of small basis set superposition error compared to Gaussian basis sets. *J. Comput. Chem.* **2008**, *29*, 225–232. [CrossRef]
16. Delley, B. Ground-state enthalpies: Evaluation of electronic structure approaches with emphasis on the density functional method. *J. Phys. Chem. A* **2006**, *110*, 13632–13639. [CrossRef] [PubMed]

17. Berisha, A. First principles details into the grafting of aryl radicals onto the free-standing and borophene/Ag(1 1 1) surfaces. *Chem. Phys.* **2021**, *544*, 111124. [CrossRef]
18. Thaçi, V.; Hoti, R.; Berisha, A.; Bogdanov, J. Corrosion study of copper in aqueous sulfuric acid solution in the presence of (2E,5E)-2,5-dibenzylidenecyclopentanone and (2E,5E)-bis[(4-dimethylamino)benzylidene]cyclopentanone: Experimental and theoretical study. *Open Chem.* **2020**, *18*, 1412–1420. [CrossRef]
19. Hsissou, R.; Benhiba, F.; Abbout, S.; Dagdag, O.; Benkhaya, S.; Berisha, A.; Erramli, H.; Elharfi, A. Trifunctional epoxy polymer as corrosion inhibition material for carbon steel in 1.0 M HCl: MD simulations, DFT and complexation computations. *Inorg. Chem. Commun.* **2020**, *115*, 107858. [CrossRef]
20. Hsissou, R.; Abbout, S.; Seghiri, R.; Rehioui, M.; Berisha, A.; Erramli, H.; Assouag, M.; Elharfi, A. Evaluation of corrosion inhibition performance of phosphorus polymer for carbon steel in [1 M] HCl: Computational studies (DFT, MC and MD simulations). *J. Mater. Res. Technol.* **2020**, *9*, 2691–2703. [CrossRef]
21. Hsissou, R.; Dagdag, O.; Abbout, S.; Benhiba, F.; Berradi, M.; El Bouchti, M.; Berisha, A.; Hajjaji, N.; Elharfi, A. Novel derivative epoxy resin TGETET as a corrosion inhibition of E24 carbon steel in 1.0 M HCl solution. Experimental and computational (DFT and MD simulations) methods. *J. Mol. Liq.* **2019**, *284*, 182–192. [CrossRef]
22. Dagdag, O.; Berisha, A.; Safi, Z.; Hamed, O.; Jodeh, S.; Verma, C.; Ebenso, E.E.; El Harfi, A. DGEBA-polyaminoamide as effective anti-corrosive material for 15CDV6 steel in NaCl medium: Computational and experimental studies. *J. Appl. Polym. Sci.* **2020**, *137*, 48402. [CrossRef]
23. Dagdag, O.; Hsissou, R.; El Harfi, A.; Berisha, A.; Safi, Z.; Verma, C.; Ebenso, E.E.; Touhami, M.E.; El Gouri, M. Fabrication of polymer based epoxy resin as effective anti-corrosive coating for steel: Computational modeling reinforced experimental studies. *Surf. Interfaces* **2020**, *18*, 100454. [CrossRef]
24. Sun, H.; Jin, Z.; Yang, C.; Akkermans, R.L.; Robertson, S.H.; Spenley, N.A.; Miller, S.; Todd, S.M. COMPASS II: Extended coverage for polymer and drug-like molecule databases. *J. Mol. Model.* **2016**, *22*, 47. [CrossRef]
25. El Faydy, M.; Benhiba, F.; Berisha, A.; Kerroum, Y.; Jama, C.; Lakhrissi, B.; Guenbour, A.; Warad, I.; Zarrouk, A. An experimental-coupled empirical investigation on the corrosion inhibitory action of 7-alkyl-8-Hydroxyquinolines on C35E steel in HCl electrolyte. *J. Mol. Liq.* **2020**, *317*, 113973. [CrossRef]
26. Dagdag, O.; Hsissou, R.; Berisha, A.; Erramli, H.; Hamed, O.; Jodeh, S.; El Harfi, A. Polymeric-Based Epoxy Cured with a Polyaminoamide as an Anticorrosive Coating for Aluminum 2024-T3 Surface: Experimental Studies Supported by Computational Modeling. *J. Bio-Tribo-Corros.* **2019**, *5*, 58. [CrossRef]
27. Dagdag, O.; Hsissou, R.; El Harfi, A.; Safi, Z.; Berisha, A.; Verma, C.; Ebenso, E.E.; Quraishi, M.A.; Wazzan, N.; Jodeh, S.; et al. Epoxy resins and their zinc composites as novel anti-corrosive materials for copper in 3% sodium chloride solution: Experimental and computational studies. *J. Mol. Liq.* **2020**, *315*, 113757. [CrossRef]
28. Jessima, S.H.M.; Berisha, A.; Srikandan, S.S.; Subhashini, S. Preparation, characterization, and evaluation of corrosion inhibition efficiency of sodium lauryl sulfate modified chitosan for mild steel in the acid pickling process. *J. Mol. Liq.* **2020**, *320*, 114382. [CrossRef]
29. Hsissou, R.; Benzidia, B.; Rehioui, M.; Berradi, M.; Berisha, A.; Assouag, M.; Hajjaji, N.; Elharfi, A. Anticorrosive property of hexafunctional epoxy polymer HGTMDAE for E24 carbon steel corrosion in 1.0 M HCl: Gravimetric, electrochemical, surface morphology and molecular dynamic simulations. *Polym. Bull.* **2020**, *77*, 3577–3601. [CrossRef]
30. El Arrouji, S.; Karrouchi, K.; Berisha, A.; Alaoui, K.I.; Warad, I.; Rais, Z.; Radi, S.; Taleb, M.; Zarrouk, A. New pyrazole derivatives as effective corrosion inhibitors on steel-electrolyte interface in 1 M HCl: Electrochemical, surface morphological (SEM) and computational analysis. *Colloids Surf. A Physicochem. Eng. Asp.* **2020**, *604*, 125325. [CrossRef]
31. Abbout, S.; Zouarhi, M.; Chebabe, D.; Damej, M.; Berisha, A.; Hajjaji, N. Galactomannan as a new bio-sourced corrosion inhibitor for iron in acidic media. *Heliyon* **2020**, *6*, e03574. [CrossRef]
32. Jarray, A.; Gerbaud, V.; Hemati, M. Polymer-plasticizer compatibility during coating formulation: A multi-scale investigation. *Prog. Org. Coat.* **2016**, *101*, 195–206. [CrossRef]
33. Klamt, A. The COSMO and COSMO-RS solvation models. *Wiley Interdiscip. Rev. Comput. Mol. Sci.* **2018**, *8*, e1338. [CrossRef]
34. Berisha, A. Experimental, Monte Carlo and Molecular Dynamic Study on Corrosion Inhibition of Mild Steel by Pyridine Derivatives in Aqueous Perchloric Acid. *Electrochem* **2020**, *1*, 188–199. [CrossRef]
35. Berisha, A. The influence of the grafted aryl groups on the solvation properties of the graphyne and graphdiyne—A MD study. *Open Chem.* **2019**, *17*, 703–710. [CrossRef]
36. Ongari, D.; Boyd, P.G.; Kadioglu, O.; Mace, A.K.; Keskin, S.; Smit, B. Evaluating Charge Equilibration Methods to Generate Electrostatic Fields in Nanoporous Materials. *J. Chem. Theory Comput.* **2019**, *15*, 382–401. [CrossRef] [PubMed]
37. Hsissou, R.; Abbout, S.; Berisha, A.; Berradi, M.; Assouag, M.; Hajjaji, N.; Elharfi, A. Experimental, DFT and molecular dynamics simulation on the inhibition performance of the DGDCBA epoxy polymer against the corrosion of the E24 carbon steel in 1.0 M HCl solution. *J. Mol. Struct.* **2019**, *1182*, 340–351. [CrossRef]
38. Mehmeti, V.; Podvorica, F.I. Experimental and Theoretical Studies on Corrosion Inhibition of Niobium and Tantalum Surfaces by Carboxylated Graphene Oxide. *Materials* **2018**, *11*, 893. [CrossRef] [PubMed]
39. Molhi, A.; Hsissou, R.; Damej, M.; Berisha, A.; Thaçi, V.; Belafhaili, A.; Benmessaoud, M.; Labjar, N.; El Hajjaji, S. Contribution to the corrosion inhibition of C38 steel in 1 M hydrochloric acid medium by a new epoxy resin PGEPPP. *Int. J. Corros. Scale Inhib.* **2021**, *10*, 399–418.

40. Dagdag, O.; Berisha, A.; Safi, Z.; Dagdag, S.; Berrani, M.; Jodeh, S.; Verma, C.; Ebenso, E.E.; Wazzan, N.; El Harfi, A. Highly durable macromolecular epoxy resin as anticorrosive coating material for carbon steel in 3% NaCl: Computational supported experimental studies. *J. Appl. Polym. Sci.* **2020**, *137*, 49003. [CrossRef]
41. Berisha, A. Ab inito exploration of nanocars as potential corrosion inhibitors. *Comput. Theor. Chem.* **2021**, *1201*, 113258. [CrossRef]
42. Uppalapati, P.K.; Berisha, A.; Velmurugan, K.; Nandhakumar, R.; Khosla, A.; Liang, T. Salen type additives as corrosion mitigtor for Ni–W alloys: Detailed electronic/atomic-scale computational illustration. *Int. J. Quantum Chem.* **2020**, *12*, e26600. [CrossRef]
43. Jessima, S.H.M.; Subhashini, S.; Berisha, A.; Oral, A.; Srikandan, S.S. Corrosion mitigation performance of disodium EDTA functionalized chitosan biomacromolecule—Experimental and theoretical approach. *Int. J. Biol. Macromol.* **2021**, *178*, 477–491. [CrossRef]
44. Dagdag, O.; Berisha, A.; Mehmeti, V.; Haldhar, R.; Berdimurodov, E.; Hamed, O.; Jodeh, S.; Lgaz, H.; El-Sayed, M.S.; Elbenso, E.E. Epoxy coating as effective anti-corrosive polymeric material for aluminum alloys: Formulation, electrochemical and computational approaches: Computational and experimental studies. *J. Mol. Liq.* **2021**, 117886. [CrossRef]
45. Dagdag, O.; El Harfi, A.; El Gana, L.; Safi, Z.S.; Guo, L.; Berisha, A.; Verma, C.; Ebenso, E.E.; Wazzan, N.; El Gouri, M. Designing of phosphorous based highly functional dendrimeric macromolecular resin as an effective coating material for carbon steel in NaCl: Computational and experimental studies. *J. Appl. Polym. Sci.* **2021**, *138*, 49673. [CrossRef]
46. Oukhrib, R.; Abdellaoui, Y.; Berisha, A.; Abou Oualid, H.; Halili, J.; Jusufi, K.; El Had, M.A.; Bourzi, H.; El Issami, S.; Asmary, F.A.; et al. DFT, Monte Carlo and molecular dynamics simulations for the prediction of corrosion inhibition efficiency of novel pyrazolylnucleosides on Cu(111) surface in acidic media. *Sci. Rep.* **2021**, *11*, 3771. [CrossRef] [PubMed]
47. Alahiane, M.; Oukhrib, R.; Berisha, A.; Albrimi, Y.A.; Akbour, A.A.E.; Hamed, O.; Oualid, H.A.S.; Bourzi, H.; Assabbane, A.; Nahlé, A.; et al. Electrochemical, thermodynamic and molecular dynamics studies of some benzoic acid derivatives on the corrosion inhibition of 316 stainless steel in HCl solutions. *J. Mol. Liq.* **2021**, *328*, 115413. [CrossRef]
48. Yu, L.J.; Zhang, J.; Qiao, G.M.; Yan, Y.G.; Ti, Y.; Zhang, Y. Effect of alkyl chain length on inhibition performance of imidazoline derivatives investigated by molecular dynamics simulation. *Mater. Corros.* **2013**, *64*, 225–230. [CrossRef]